ACS SENSORS

pubs.acs.org/acssensors Article

Discriminating BTX Molecules by the Nonselective Metal Oxide Sensor-Based Smart Sensing System

Hongyu Liu, Gang Meng,* Zanhong Deng, Kazuki Nagashima, Shimao Wang, Tiantian Dai, Liang Li,* Takeshi Yanagida, and Xiaodong Fang*

Cite This: https://doi.org/10.1021/acssensors.1c01704 Read Online

ACCESS | Metrics & More | Article Recommendations | Supporting Information

ABSTRACT: Discriminating structurally similar volatile organic compounds (VOCs) molecules, such as benzene, toluene, and three xylene isomers (BTX), remains a significant challenge, especially, for metal oxide semiconductor (MOS) sensors, in which selectivity is a long-standing challenge. Recent progress indicates that temperature modulation of a single MOS sensor offers a powerful route in extracting the features of adsorbed gas analytes than conventional isothermal operation. Herein, a rectangular heating waveform is applied on NiO-, WO_3-, and SnO_2-based sensors to gradually activate the specific gas/oxide interfacial redox reaction and generate rich (electrical) features of adsorbed BTX molecules. Upon several signal preprocessing steps, the intrinsic feature of BTX molecules can be extracted by the linear discrimination analysis (LDA) or convolutional neural network (CNN) analysis. The combination of three distinct MOS sensors noticeably benefits the recognition accuracy (with a reduced number of training iterations). Finally, a prototype of a smart BTX recognition system (including sensing electronics, sensors, Wi-Fi module, UI, PC, etc.) based on temperature modulation has been explored, which enables a prompt, accurate, and stable identification of xylene isomers in the ambient air background and raises the hope of innovating the future advanced machine olfactory system.

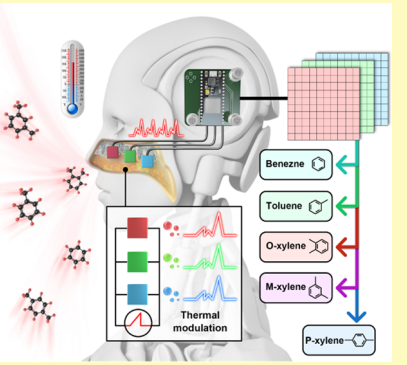

KEYWORDS: *BTX molecules, xylene isomer classification, temperature modulation, deep learning algorithm, smart sensing system*

BTX, referring to benzene, toluene, and three xylene isomers (including *m*-xylene, *o*-xylene, and *p*-xylene), are very important petrochemical agents used as either raw material or solvent. With the accelerated consumption of BTX aromatic hydrocarbons in the printing, paint, rubber, polymer, leather, and pharmaceuticals industries, as well as rapid popularization of vehicles, a large amount of BTX-based volatile organic compounds (VOCs) have been emitted into the environments and constitute one kind of most alarming indoor and outdoor air pollution sources.[1,2] Apart from most hazardous benzene (class 1 human carcinogen), exposure to toluene and xylene also severely impairs the human blood production process and nervous system, depending on the exposure concentration and time. The permissible exposure limit (PEL), recommended by US National Institute for Occupational Safety and Health, for benzene, toluene, and xylene as the 8 h time-weighted average (TWA) is 0.1, 100, and 100 ppm, respectively.[3] The toxicity effects (as well as applications) of BTX closely relate with their slight structural difference, even for xylene isomers.[4,5] Thus, exploring a facile distinction methodology is of utmost importance.

Though gas chromatography−mass spectrometry (GC-MS) or gas chromatography-flame ionization detector (GC-FID) enables the discrimination of BTX species, high cost, low efficiency of these bulk instruments, and high requirement for the operators hinder the widespread applications.[6] The forthcoming trillion sensor society calls for smart sensing systems, which could not only promptly warn the risk of exceeding PEL concentrations but also help to identify the pollution source, with the assistance of Internet of Things (IoT). In this regard, semiconductor (carbon nanotubes, metal sulfide andoxides) sensors[5,7−9] outperform the other kinds of portable sensors (optical waveguide/fluorescence,[10,11] quartz crystal microbalance (QCM)[12]), in terms of excellent silicon chip compatibility, direct electrical readout, ultralow cost and dimension.[13] Nevertheless, till now, it remains a significant challenge to discriminate five BTX molecules by semiconductor (as well as other portable) sensors, arising from both intrinsically poor selectivity of semiconductor sensors and quite similar physical properties (including kinetic diameter,[14] ionization potential,[15] dipole moment, etc.) of BTX molecules, as listed in Table S1.

Semiconductor sensors were usually operated at an elevated (isothermal) temperature to observe a clear resistance/conductance variation upon exposure to target molecules;

Received: August 11, 2021
Accepted: October 22, 2021

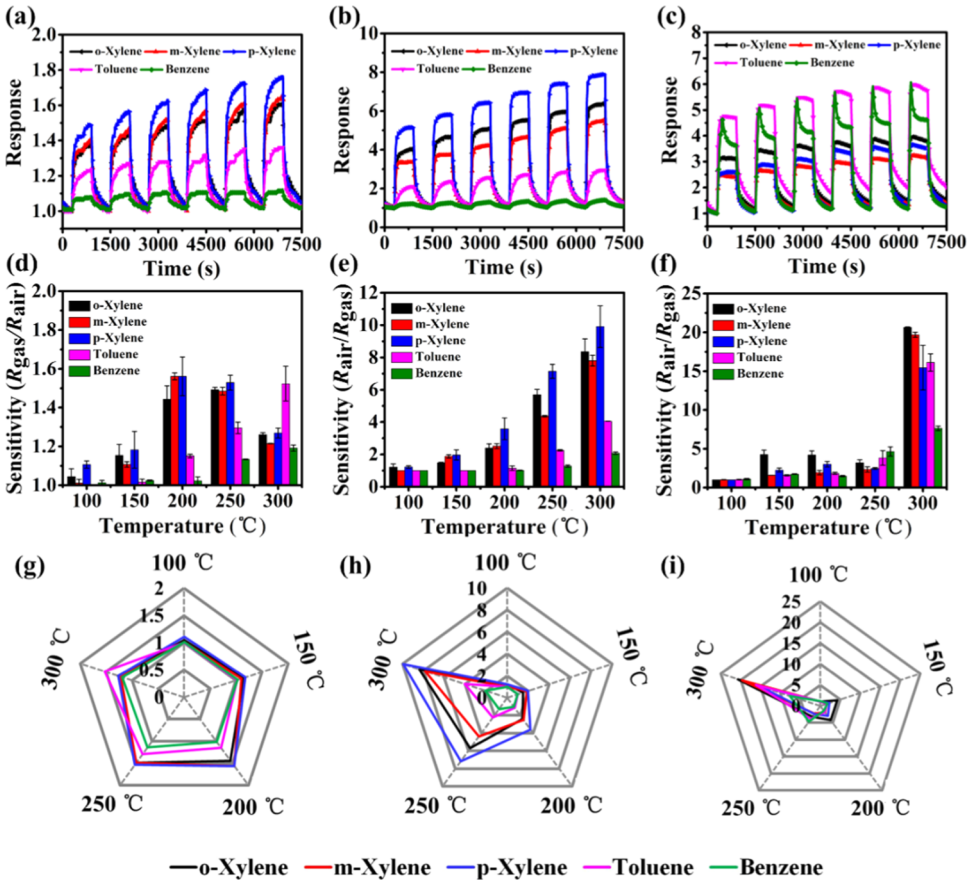

Figure 1. Isothermal responses of NiO, WO_3, and SnO_2 sensors to *o*-xylene, *m*-xylene, *p*-xylene, toluene, and benzene vapors. Variations of (a) NiO, (b) WO_3, and (c) SnO_2 sensors response upon successive exposure to various BTX vapors (30−80 ppm) at a working temperature of 250 °C. (d−f) Histogram and (g−i) radar plots of NiO, WO_3, and SnO_2 sensor sensitivity to 100 ppm various BTX vapors, as a function of the working temperature ranging from 100 to 300 °C.

isothermal sensitivity was typically extracted as one "feature" of target molecules. Resembling with face/fingerprint recognition, extracting sufficient features of target molecules from electrical response signals is necessary.[16,17] Modifying the surface properties of sensors by doping,[18,19] decoration,[8,20] or hybridization offers an apparent approach of expanding features of target molecules by constructing sensor arrays.[21−24] Wang et al. reported an efficient approach to extract molecule features by analyzing multiple field-effect transistor (FET) characteristics of an ambipolar diketopyrrolopyrrole (DPP) copolymer sensor, and discrimination of three xylene isomers (a fixed concentration of 40 ppm in the inert N_2 background) was first demonstrated.[5] However, insufficient stabilities in the structure (i.e., swelling) and electrical properties of DPP in the ambient air atmosphere hinder its practical applications.[25] A robust smart sensing system enabling fast identification of BTX molecules in an air atmosphere is still lacking.

Instead of limited features extracted from isothermal (resistance or FET) measurements,[6,8,11,26] transient response signals from a temperature-modulated sensor were adopted.[27−29] As the binding states of different adsorbed molecules on the specific facets of a sensor surface are different and possess unique thermodynamic characteristics, the temperature-modulated transient signals probably contain both unique thermodynamic and kinetic information of adsorbed molecules. Herein, a rectangular heating waveform (from 150 to 250 °C) was applied on generic, nonselective MOS (NiO-, WO_3-, and commercial SnO_2-based TGS 2602) sensors. Through necessary signal preprocessing steps, the intrinsic features of exposure gas analytes can be extracted either by the linear discrimination analysis (LDA) or convolutional neural network (CNN) analysis. By virtue of the distinct surface chemical properties of three oxides, the entire sensors possess better discrimination capability (suggested by the LDA) and fast training convergence characteristics (revealed by CNN). Finally, a smart sensing system, including a compact temperature modulation and resistance reading module (6 × 6 cm^2), Wi-Fi module, user interface (UI), and PC server, has been constructed, which enables a prompt (∼5 s) discrimination of xylene isomer vapors with the same molecular weight and functional group. Moreover, owing to the excellent stability of these MOS sensors in the ambient air atmosphere below 250 °C, the present thermally modulated sensing electronics exhibit robust discrimination capability (a slight shift of base resistance does not account for the shift of a feature space). This work highlights that appropriate thermal modulation offers a powerful route in extracting the feature differences of highly similar molecules like BTX, including xylene isomers, and the recent advancement in deep learning algorithms in the area of artificial intelligence (AI) could substantially empower the recognition capability of nonselective semiconductor sensors. The combination of two strengths promises the innovation of intelligent molecule recognition chips for the future machine olfaction.

https://doi.org/10.1021/acssensors.1c01704
ACS Sens. XXXX, XXX, XXX−XXX

RESULTS AND DISCUSSION

The TEM images of as-synthesized NiO and WO_3 products are shown in Figure S1a,b, and both materials reveal homogeneous nanoparticles with different size ranges. The grain size of NiO nanoparticles was 21.3 ± 6.0 nm (inset of Figure S1a) and that of WO_3 nanoparticles was 43.4 ± 12.5 nm (inset of Figure S1b). SAED (inset of Figure S1c,d) and EDS (Figure S1e,f) characterization confirms the pure cubic phase of NiO nanoparticles and the monoclinic phase of WO_3 nanoparticles, respectively. To compare the electrical responses of NiO, WO_3, and SnO_2 sensors to five BTX vapors and gain an insight into the differences of BTX molecules/MOS interfacial charge interaction, the isothermal response characteristics are first investigated. The successive sensitivity (R_{gas}/R_{air} for p-type NiO, R_{air}/R_{gas} for n-type WO_3 and SnO_2) response and recovery curves of the three sensors to the tested BTX vapors (30−80 ppm) at an operating temperature of 250 °C are shown in Figure 1a−c. All of the MOS sensors show the cross-sensitivity to *o*-xylene, *m*-xylene, *p*-xylene, toluene, and benzene vapors, and their sensitivity response curves exhibit a similar response profile, except for the benzene response of the SnO_2 sensor. The appearance of oscillation at an elevated operating temperature (250 °C) probably arises from the local temperature increase of the SnO_2 sensor induced by exothermic oxidation of exposure to benzene.[28] The three sensors exhibit differential sensitivities and response kinetics, which should be due to the distinct surface chemical properties of the sensing material. As shown in Figure 1a−c, the sensitivity response values of NiO, WO_3, and SnO_2 sensors in various BTX atmospheres range from 1.08 to 1.76, 1.21 to 7.90, and 2.41 to 6.00, respectively, which suggest the nonspecific nature of present sensors.

Because the resistance (R) of the sensor gradually varies (increase for NiO, decrease for WO_3 and SnO_2) with the concentration or partial pressure (P) variation of BTX gas, the sensor sensitivity usually increases gradually with the increase of gas concentration. The sensitivity response follows the power law, and its constant relates to the interaction mode between the target gas and the reactive oxygen species on the MOS surface. The p-type NiO sensor possesses lower sensitivity than WO_3 and SnO_2 sensors because of its low carrier mobility and hole accumulation configuration.[26] For all of the sensors, the operating temperature plays an important role in modulating the electrical responses, as shown by the temperature-dependent responses to 100 ppm BTX vapors in Figure 1d−f. The response of the sensor typically increases first and then decreases with the increase of the operating temperature, as shown in Figure 1d. The main reason for this phenomenon is that the rate constant (k_R) of the reaction between the gas and the adsorbed oxygen increases exponentially with the increase of temperature, while the change of the Knudsen diffusion coefficient (D_K) of the target gas is sublinear. The rate constant k_R is less than D_K in the lower temperature region and greater than D_K in the higher temperature region. With the increase of temperature, the gas inside the porous sensing layer is consumed in large quantities. The effective partial pressure (P_{in}) of gas inside the material is significantly lower than that outside (P_{out}), and the actual sensitivity response decreases with increasing temperature at high temperatures. Therefore, the aperture size and the diffusion length of the MOS are also factors that affect the gas sensitivity response in the high-temperature region. In addition, the adsorption oxygen content of the MOS surface decreased with the increase of temperature. When the concentration (partial pressure) of the target gas is too high, the adsorption oxygen is consumed and the gas response decreases with the increase of temperature. In summary, the sensitivity at different operating temperatures is affected not only by the type of target gas and MOS but also by the device structure, sensing material morphology and surface reactive oxygen species. The different temperature-dependent response characteristics in the radar plot (Figure 1g−i) suggest the differences in terms of BTX molecular diffusion, molecular adsorption, and high-temperature activation at different operating temperatures. The formula of the Knudsen diffusion coefficient (D_K) of gas is as follows ($\bar{r}$ is the aperture, T is the temperature, and M_A is the molecular weight of the gas)

$$D_K = 9700\bar{r}\sqrt{\frac{T}{M_A}} \tag{1}$$

which is different for benzene, toluene, and xylene with different molecular weights. Meanwhile, overcoming activation energy (E_a) is the premise for the redox process on the surfaces of MOS and gas. The formula of activation energy is as follows (N_s is the density of negative surface charge, N_d is the density of positive charge, ε_r is the dielectric constant of the semiconductor, ε_0 is the dielectric constant of gas, and q is the basic charge)

$$E_a = \frac{q^2 N_s^2}{2\varepsilon_r \varepsilon_0 N_d} \tag{2}$$

The chemical reaction rate (k_R) is closely related to the activation energy (the lower the activation energy, the faster the reaction rate). The formula of the reaction rate constant k_R is as follows (R is the gas constant, T is the temperature, and A is the pre-exponential factor)

$$k_R = Ae^{-E_a/RT} \tag{3}$$

According to Table S1, the dielectric constant of BTX gases is different, and the redox rate constant k_R of different BTX gases on the MOS surface is different. By changing the operation temperature of the sensor, the features of temperature-dependent rate constants such as the rate constant (k_R) of the redox reaction and the Knudsen diffusion coefficient (D_K) of the gas can be determined to show a promising avenue in the exploration of BTX molecule discrimination.

The parameters of thermal modulation, such as waveform, range, and period, play a crucial role on the amount of molecular information contained in the dynamic response curves. A simple rectangular heating wave (red line in Figure 2) is applied to achieve the fastest recognition at a moderate operation condition. Considering low sensitivity at low temperature and larger energy consumption at high temperatures of the sensors (Figure 1d−f), the temperature of the sensor was modulated from 150 to 250 °C by increasing the heating voltage. Note that there is a thin ceramic insulator (1.5 × 1.5 × 0.25 mm^3) between the top MOS sensing layer and bottom heating layer, and the temperature of the top sensing layer gradually increases to 250 °C (to gradually activate the surface redox reaction). Using the inherent temperature coefficient of resistance/resistivity (TCR) characteristics of the MOS channel, the transient resistance of the three sensors under the rectangular wave heating waveform was monitored

https://doi.org/10.1021/acssensors.1c01704
ACS Sens. XXXX, XXX, XXX−XXX

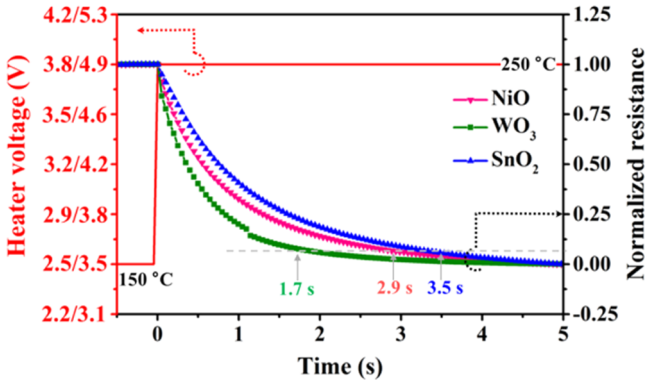

Figure 2. Rectangular thermal modulation waveform and transient sensor normalized resistances (with respect to the resistance at 150 °C) of NiO, WO_3, and SnO_2 sensors (in dry air).

under dry air atmosphere, and the thermal response times (the time for reaching 90% of temperature increase) of NiO, WO_3, and SnO_2 sensors were about 2.9, 1.7, and 3.5 s, respectively. The difference in the thermal response time arises from different specific heats and thermal conductivities of the MOS sensing layer. A thermal modulation period of 5 s (Figure 2) was used for subsequent experiments.

After the thermal modulation testing, the original signal (response resistance) and the subsequent signal processing procedure of NiO, WO_3, and SnO_2 sensors can be seen in Figures S2−S4, respectively. A signal preprocessing method described in the SI and our previous work[28] was applied to eliminate redundant signals from the original signals. As shown in Figure 3, after getting rid of TCR interferences, removing concentration-related information and suppressing noise information step by step, the extracted signal profiles were analyzed by the LDA (Figure 4). Though using the discrete wavelet transform (DWT) derived signals (Figure 4d−f) allows for better discrimination than the untreated signals (Figure 4a−c), overlapping of features occurs for all of the individual sensors, for example, partial overlapping of benzene and toluene for the NiO sensor, mixing of benzene and toluene or *o*-xylene and *m*-xylene for the WO_3 sensor, and overlapping of *m*-xylene, *p*-xylene, and toluene for the SnO_2 sensor. Based on the 70 sets of validation responses recorded at the parallel independent experimental sessions for all BTX vapors (filled markers in Figure 4), the accuracy of NiO, WO_3, and SnO_2 sensors in the identification of BTX vapors is 97.14, 90.00, and 97.14%, respectively. The discrepancy of recognition capability agrees with the fact that MOS sensors belong to chemical sensors, in which the electrical response arises from the specific (temperature-dependent) surface redox reactions at the gas/MOS interface. A slight variation of the sensing material may degrade the discrimination capability even using thermal modulation, as indicated by the results of SnO_2-based TGS 2600, 2602, and 2603 (Figure S5). The selection of the appropriate sensing material toward the specific target analyte is another interesting work beyond the scope of this work. Enlarging the number of distinct MOS sensors or combining the temperature-modulated features of NiO (p-type 3d oxide, with outstanding VOCs catalytic oxidation properties[30,31]), WO_3 (n-type 5d oxide), and commercial SnO_2-based VOCs sensors (TGS 2602) can clearly discriminate the five BTX molecules, with 100% recognition and the classification rate, as shown in Figure 5.

As for the core of thermal modulation, the feature extraction method has always been reported using time−frequency transformation technology,[29,32,33] transforming the signals from the time domain to the frequency domain, in which localized frequency signals have been extracted as the distinguishable features related to the gas molecules. However, the selection of "localized frequency signal" is always result-oriented and subjectively selected, thus hinders the way to design the smart gas identification system. To use a more objective denoising method to achieve BTX gas classification

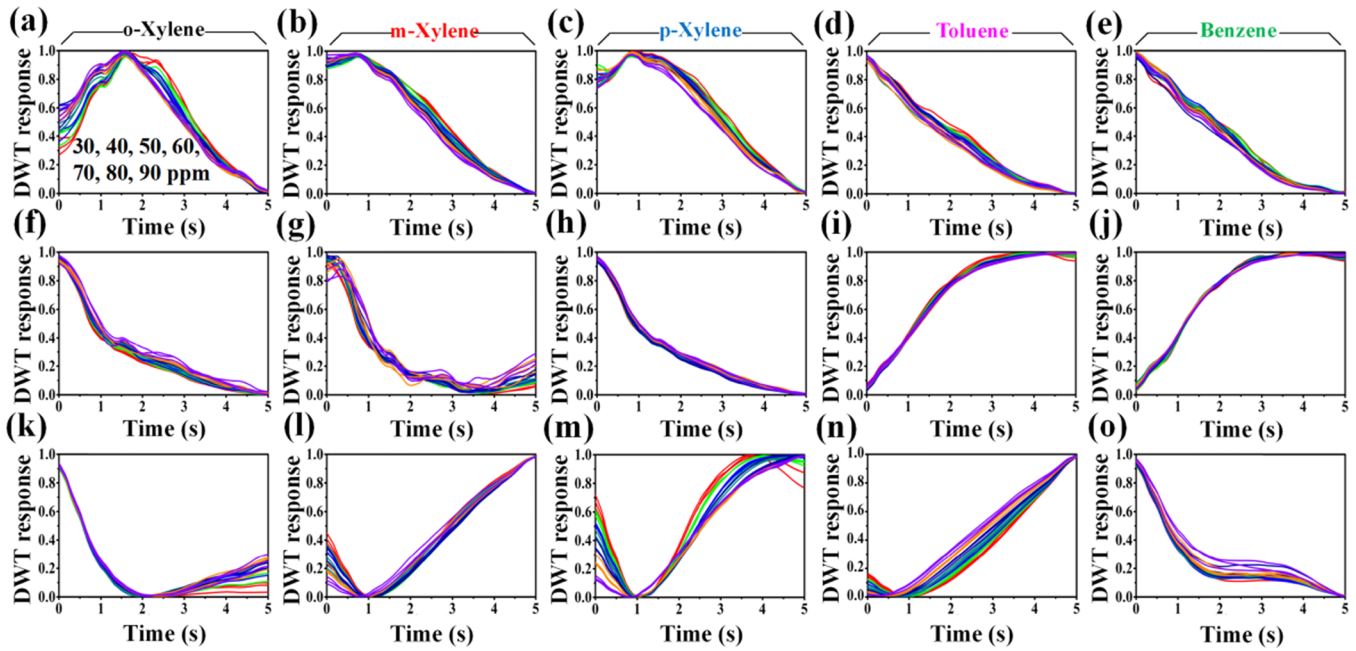

Figure 3. DWT response of (a−e) NiO, (f−j) WO_3, and (k−o) SnO_2 sensors to five kinds of BTX vapors each at different concentrations in the range of 30−90 ppm.

https://doi.org/10.1021/acssensors.1c01704
ACS Sens. XXXX, XXX, XXX−XXX

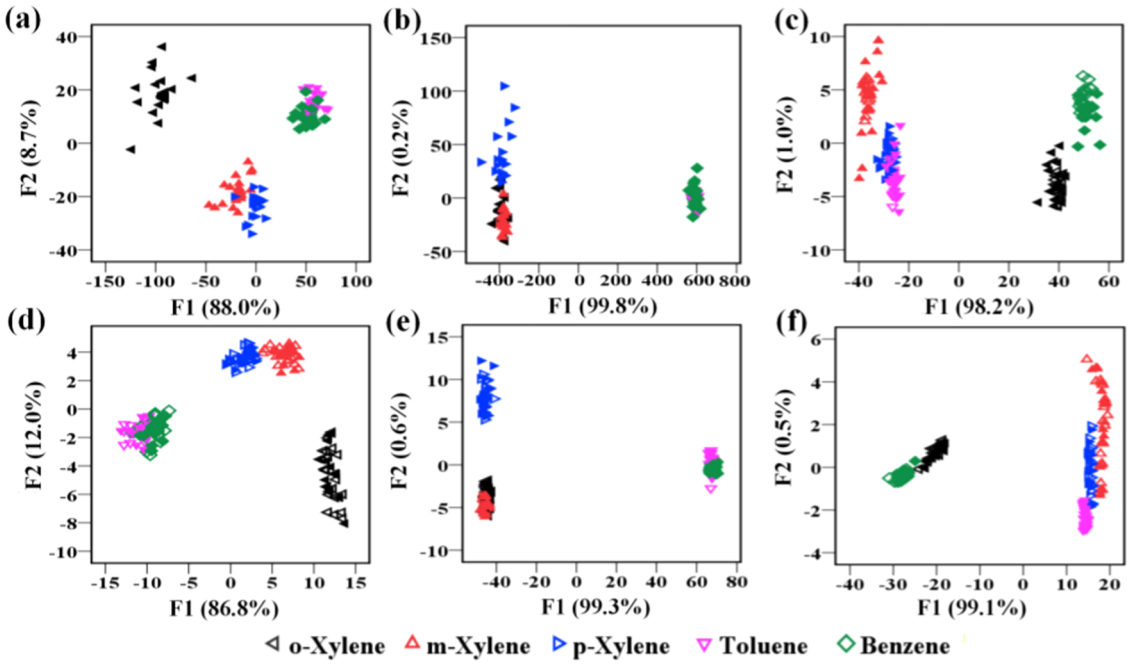

Figure 4. LDA feature space of (a) NiO, (b) WO_3, and (c) SnO_2 sensor response patterns using the normalized thermal modulation sensitivity response signals. LDA mapping of (d) NiO, (e) WO_3, and (f) SnO_2 sensor response patterns using the DWT dirived signals. Filled markers present verification tests carried out in the independent experimental session.

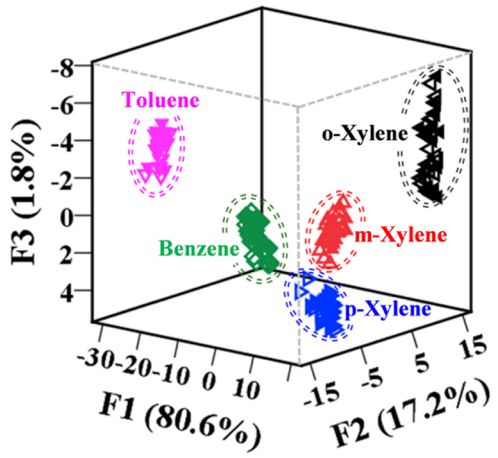

Figure 5. 3D feature space of LDA-derived scatter plot using preprocessed response signals of NiO, WO_3, and SnO_2 sensors together. Filled markers present verification tests carried out in the independent experimental session.

and identification only by a single sensor, a deep learning-based conceptual design, CNN, was explored to analyze and recognize BTX vapors (Figure S6). It is known the BPNN has not only good noise tolerance but also excellent robustness.[34,35] CNN is developed on the basis of back-propagation neural network (BPNN), which consists of two parts: feature extraction and data dimensionality reduction neural network composed of a convolutional layer, a pooling layer, and a classification neural network composed of BPNN.[36,37] With the characteristics and advantages of BPNN, the CNN model should also be used as a direct learning filter instead of DWT for feature extraction, transforming the artificial feature extraction into automatic feature extraction with implicit self-learning.

First, the learning rate of the CNN is investigated because it determines the distance of weight moving in the gradient direction in each batch. With a high learning rate, training may not converge at all, or even diverge. The change in weight can be so large that the optimization oversteps the minimum value of the loss function. When the learning rate is low, each step approaching the minimum value of the loss function is small. Although the training becomes more reliable, the optimization will take a long time. The cross entropy of CNN for different learning rates is shown in Figure S7. The learning rate starts at a value like 0.1 and then drops exponentially, such as 0.01 and 0.001, to estimate the learning rate that optimizes the value of the loss function without losing the training speed. The results show that the learning rate of 0.01 compromises between the minimum cross entropy and the training speed. Figure S7c illustrates the cross entropy of CNN with a different number of neurons in the fully connected layers and the error bars demonstrate that the CNN was trained at different initial states. For simplicity, the two fully connected layers have an equal number of neurons, and the results show that the cross entropy decreases with the increasing number of neurons and subsequently levels off after the number of neurons above 200. Thus, 200 neurons will be the optimal number of nodes in the fully connected layers of CNN.

For the validation process, 105 data sets for training and 70 data sets for testing of each sensor were projected on the BPNN and the CNN, and the results are displayed in Figure 6. The cross entropy decreases with the iteration of neural network training rounds, and the accuracy of BTX identification increases with the iteration of the training. It is remarkable that compared with BPNN, the loss of CNN decreases faster, and it requires fewer training rounds to reach the maximum recognition rate. Furthermore, CNN has the best recognition accuracy by comparing the results of species identification of the four algorithms mentioned in our paper, as shown in Table 1 and Figure S8. The BTX recognition

https://doi.org/10.1021/acssensors.1c01704
ACS Sens. XXXX, XXX, XXX−XXX

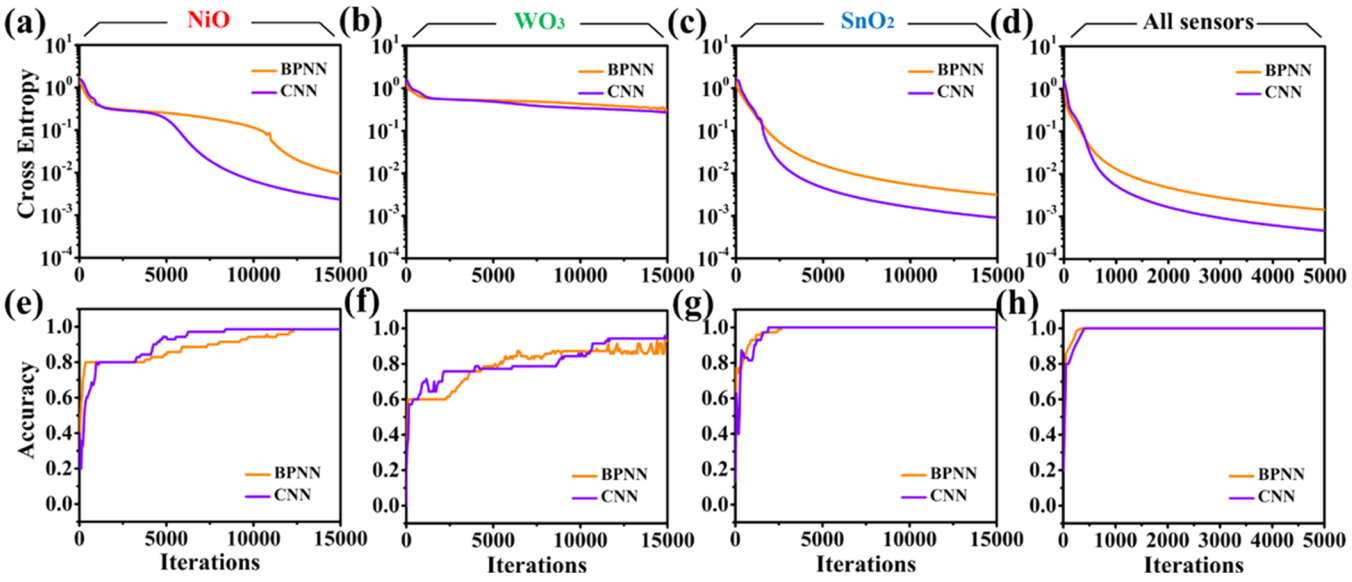

Figure 6. Comparison of cross entropy between BPNN and CNN for individual (a) NiO, (b) WO_3, (c) SnO_2, and (d) three sensors together. (e–h) Comparison of species identification accuracy.

Table 1. Accuracy of Species Identification with Four Algorithms

algorithm	NiO (%)	WO_3 (%)	SnO_2 (%)
LDA	90.00	75.71	97.14
DWT + LDA	97.14	90.00	97.14
BPNN	98.57	94.29	100
CNN	98.57	95.71	100

accuracy of NiO, WO_3, and SnO_2 sensors under the CNN algorithm is 98.57, 95.71, and 100%, respectively. Therefore, robust prompt discrimination of BTX molecules could be successfully achieved by the CNN analysis of a single sensor. In addition, it is worth noting that the recognition and classification rate of 100% BTX vapors can be achieved by combining the normalized sensitivity response signals of the three sensors, whether using BPNN or CNN. As shown in Figure 6h, when the signals of the three sensors are fed into the neural network for training together, the decreasing speed of cross entropy and the increasing speed of recognition rate are greatly improved, and it requires fewer training rounds to reach the maximum recognition rate. Therefore, it is hopeful to realize the qualitative and quantitative identification of a huge amount of complex gases with the increase of CNN depth and scale and the number of sensor arrays using the thermal modulation method.

Finally, a mini smart (temperature modulation) sensing system was designed to recognize multiple xylene isomers using a single SnO_2 gas sensor (Figure 7). The temperature modulation circuit board (Figure S9a), controlled by the PC user interface, was placed in a glass chamber (Figure S9b). Under the ambient humid air atmosphere background (relative humidity of 50–60%), three kinds of saturated xylene vapors were injected into the chamber. The temperature-modulated response signal of the sensor was simultaneously sent to the PC through a Wi-Fi module. After signal processing, as shown in Figure S10, the normalized response signal was fed into the CNN model, and the forward propagation of the parameters after training was used to identify the xylene types. As shown in Figure 8, 21 data sets of each xylene vapor were trained, and 14 data sets of each xylene vapor were fed into the CNN model for testing. The recognition accuracy of the smart sensing system was as high as 95.24%. Relative humidity is one of the crucial factors affecting the practical application of MOS sensors. Although relative humidity may affect the baseline resistance and sensitivity of MOS sensors, the influence of

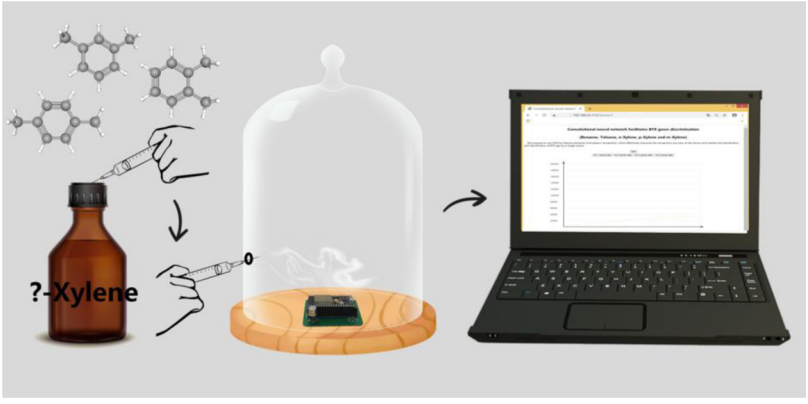

Figure 7. Schematic diagram of the smart sensing system using a single SnO_2 sensor to identify multiple xylene isomers.

https://doi.org/10.1021/acssensors.1c01704
ACS Sens. XXXX, XXX, XXX–XXX

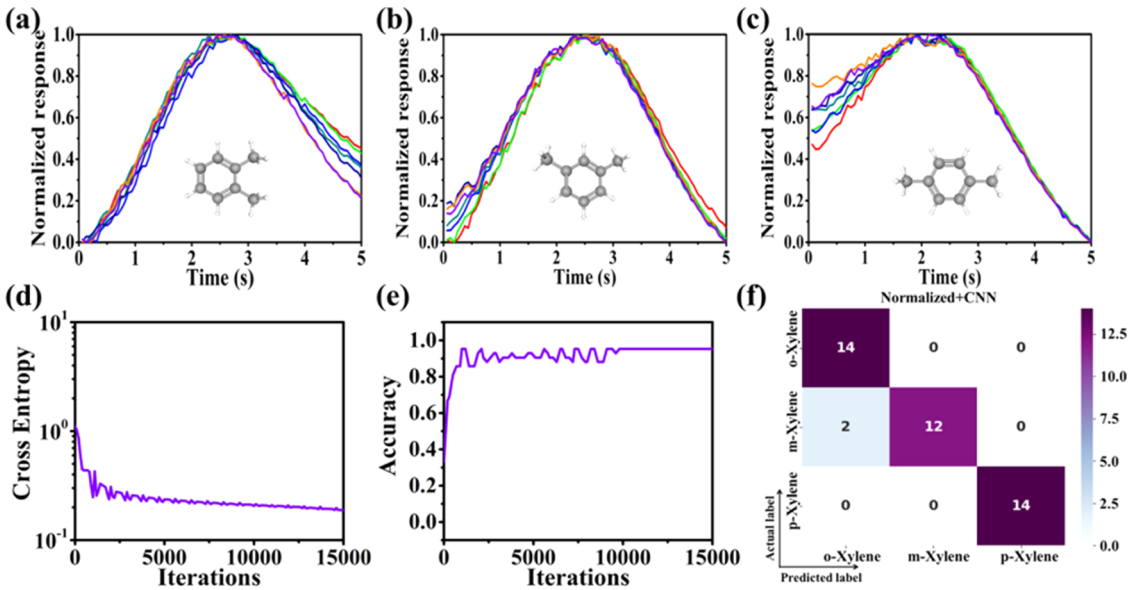

Figure 8. Smart sensing system: signal preprocessing, training, and recognition. (a–c) Normalized response signals of the SnO_2 sensor in the smart sensing system to three kinds of xylene isomer vapors (30–90 ppm). (d) Cross entropy of the system CNN changes with the increase of the number of training iterations. (e) Identification accuracy of the system CNN changes with the increase of the number of training iterations. (f) Confusion matrix of the smart sensing system using a single SnO_2 sensor to identify multiple xylene isomer vapors.

relative humidity on $R(t)$ and $S(t)$ of the sensor is synchronous, and therefore, it has negligible influence on the recognition features (Figure S11). Moreover, because of the material robustness of MOS in the ambient (humid) air atmosphere and the response signal preprocessing method, a slight shift of base resistance and the response of MOS sensors would not affect the extraction of intrinsic molecule features contained in thermal modulation response signals. We have monitored the feature pattern of xylene acquired by the present smart sensing system, and the absence of a significant feature shift and overlapping within 4 months (Figure S12) indicates excellent long-term discrimination stability. Together with good selectivity of xylene isomers with respect to three kinds of common VOCs (Figure S13), temperature modulation of sensor arrays raises the hope of the smart VOCs recognition system for diverse emerging applications.

CONCLUSIONS

Transient electrical response signals of generic nonselective MOS sensors under an appropriate temperature modulation waveform contain rich features of adsorbed gas molecules. Structurally similar BTX molecules (including three kinds of xylene isomers) can be readily discriminated by either single or multiple nonselective MOS sensor(s) with the assistance of deep learning algorithms. Together with excellent chemical and thermal stabilities of MOS in the ambient humid air atmosphere, direct electrical readout, and silicon chip compatibility, a smart sensing system based on temperature modulation is demonstrated, which enables a prompt and accurate discrimination of xylene isomer molecules and raises the hope of exploring the future smart machine olfactory system.

METHODS/EXPERIMENTAL SECTION

Experimental details are provided in the Supporting Information (SII).

ASSOCIATED CONTENT

Supporting Information

The Supporting Information is available free of charge at https://pubs.acs.org/doi/10.1021/acssensors.1c01704.

Signal preprocessing method; methods/experimental section; characterization of materials; cross entropy; confusion matrix; network structure; diagram of the measurement setup and smart machine olfactory system; and additional graphs (PDF)

AUTHOR INFORMATION

Corresponding Authors

Gang Meng − *Anhui Institute of Optics and Fine Mechanics, and Key Lab of Photovoltaic and Energy Conservation Materials, Chinese Academy of Sciences, Hefei 230031, China;* orcid.org/0000-0002-3365-8963; Email: menggang@aiofm.ac.cn

Liang Li − *School of Physical Science and Technology, Jiangsu Key Laboratory of Thin Films, Center for Energy Conversion Materials & Physics (CECMP), Soochow University, Suzhou 215006, China;* orcid.org/0000-0003-0708-7762; Email: lli@suda.edu.cn

Xiaodong Fang − *College of New Materials and New Energies, Shenzhen Technology University, Shenzhen 518118, China;* Email: fangxiaodong@sztu.edu.cn

Authors

Hongyu Liu − *College of New Materials and New Energies, Shenzhen Technology University, Shenzhen 518118, China; Guangdong Key Laboratory for Biomedical Measurements and Ultrasound Imaging, School of Biomedical Engineering, Shenzhen University Health Science Center, Shenzhen 518060, China*

Zanhong Deng − *Anhui Institute of Optics and Fine Mechanics, and Key Lab of Photovoltaic and Energy Conservation Materials, Chinese Academy of Sciences, Hefei 230031, China;* orcid.org/0000-0003-3487-9167

https://doi.org/10.1021/acssensors.1c01704
ACS Sens. XXXX, XXX, XXX−XXX

Kazuki Nagashima − *Department of Applied Chemistry, Graduate School of Engineering, The University of Tokyo, Tokyo 113-8656, Japan;* orcid.org/0000-0003-0180-816X

Shimao Wang − *Anhui Institute of Optics and Fine Mechanics, and Key Lab of Photovoltaic and Energy Conservation Materials, Chinese Academy of Sciences, Hefei 230031, China;* orcid.org/0000-0002-4495-6130

Tiantian Dai − *Anhui Institute of Optics and Fine Mechanics, and Key Lab of Photovoltaic and Energy Conservation Materials, Chinese Academy of Sciences, Hefei 230031, China*

Takeshi Yanagida − *Department of Applied Chemistry, Graduate School of Engineering, The University of Tokyo, Tokyo 113-8656, Japan;* orcid.org/0000-0003-4837-5701

Complete contact information is available at: https://pubs.acs.org/10.1021/acssensors.1c01704

Notes

The authors declare no competing financial interest.

■ ACKNOWLEDGMENTS

This research was financially supported by the CAS Pioneer Hundred Talents Program from Chinese Academy of Sciences, National Natural Science Foundation of China (52025028, 11674324, and 62075223), Natural Science Foundation of Top Talent of SZTU (2020101), and CAS-JSPS Joint Research Projects (GJHZ1891). The authors thank Mr. Ning Pan and Liming Fan for partial support in the circuit design.

■ REFERENCES

(1) Kang, Y.; Kim, K.; Cho, B.; Kwak, Y.; Kim, J. Highly Sensitive Detection of Benzene, Toluene, and Xylene Based on CoPP-Functionalized TiO_2 Nanoparticles with Low Power Consumption. *ACS Sensors* **2020**, *5*, 754−763.

(2) Edokpolo, B.; Yu, Q. J.; Connell, D. Health Risk Assessment of Ambient Air Concentrations of Benzene, Toluene and Xylene (BTX) in Service Station Environments. *Int. J. Environ. Res. Public Health* **2014**, *11*, 6354−6374.

(3) Barsan, M. E. *NIOSH Pocket Guide to Chemical Hazards*; National Institute for Occupational Safety and Health: USA, 2007.

(4) Elvers, B.; Hawkins, S.; Russey, W. *Ullmann's Encyclopedia of Industrial Chemistry*; Wiley-VCH: Weinheim, BW, Germany, 2011.

(5) Wang, B.; Huynh, T. P.; Wu, W. W.; Hayek, N.; Do, T. T.; Cancilla, J. C.; Torrecilla, J. S.; Nahid, M. M.; Colwell, J. M.; Gazit, O. M.; Puniredd, S. R.; McNeill, C. R.; Sonar, P.; Haick, H. A Highly Sensitive Diketopyrrolopyrrole-Based Ambipolar Transistor for Selective Detection and Discrimination of Xylene Isomers. *Adv. Mater.* **2016**, *28*, 4012−4018.

(6) Mirzaei, A.; Kim, J. H.; Kim, H. W.; Kim, S. S. Resistive-based gas sensors for detection of benzene, toluene and xylene (BTX) gases: a review. *J. Mater. Chem. C* **2018**, *6*, 4342−4370.

(7) Ndiaye, A.; Bonnet, P.; Pauly, A.; Dubois, M.; Brunet, J.; Varenne, C.; Guerin, K.; Lauron, B. Noncovalent Functionalization of Single-Wall Carbon Nanotubes for the Elaboration of Gas Sensor Dedicated to BTX Type Gases: The Case of Toluene. *J. Phys. Chem. C* **2013**, *117*, 20217−20228.

(8) Sui, L.; Zhang, X. F.; Cheng, X. L.; Wang, P.; Xu, Y. M.; Gao, S.; Zhao, H.; Huo, L. H. Au-Loaded Hierarchical MoO_3 Hollow Spheres with Enhanced Gas-Sensing Performance for the Detection of BTX (Benzene, Toluene, And Xylene) and the Sensing Mechanism. *ACS Appl. Mater. Interfaces* **2017**, *9*, 1661−1670.

(9) van den Broek, J.; Abegg, S.; Pratsinis, S. E.; Guntner, A. T. Highly selective detection of methanol over ethanol by a handheld gas sensor. *Nat. Commun.* **2019**, *10*, No. 4220.

(10) Kadir, R.; Yimit, A.; Ablat, H.; Mahmut, M.; Itoh, K. Optical Waveguide BTX Gas Sensor Based on Polyacrylate Resin Thin Film. *Environ. Sci. Technol.* **2009**, *43*, 5113−5116.

(11) Liu, X.; Gong, Y. J.; Xiong, W.; Cui, L. F.; Hu, K.; Che, Y. K.; Zhao, J. C. Highly Selective Detection of Benzene, Toluene, and Xylene Hydrocarbons Using Coassembled Microsheets with Forster Resonance Energy Transfer-Enhanced Photostability. *Anal. Chem.* **2019**, *91*, 768−771.

(12) Luo, S.-X. L.; Lin, C. J.; Ku, K. H.; Yoshinaga, K.; Swager, T. M. Pentiptycene Polymer/Single-Walled Carbon Nanotube Complexes: Applications in Benzene, Toluene, and o-Xylene Detection. *ACS Nano* **2020**, *14*, 7297−7307.

(13) Guo, S.; Yang, D.; Zhang, S.; Dong, Q.; Li, B. C.; Tran, N.; Li, Z. Y.; Xiong, Y. J.; Zaghloul, M. E. Development of a Cloud-Based Epidermal $MoSe_2$ Device for Hazardous Gas Sensing. *Adv. Funct. Mater.* **2019**, *29*, No. 1900138.

(14) Van der Perre, S.; Van Assche, T.; Bozbiyik, B.; Lannoeye, J.; De Vos, D. E.; Baron, G. V.; Denayer, J. F. M. Adsorptive Characterization of the ZIF-68 Metal-Organic Framework: A Complex Structure with Amphiphilic Properties. *Langmuir* **2014**, *30*, 8416−8424.

(15) GFG instrumentation Chemical Ionization Potential (eV) and 10.6 eV PID Correction Factors (CF). http://goodforgas.com/wp-content/uploads/2013/12/TN2004_PID_gas_table_01_16_09.pdf, accessed 6, 2021.

(16) Hierlemann, A.; Gutierrez-Osuna, R. Higher-order chemical sensing. *Chem. Rev.* **2008**, *108*, 563−613.

(17) Chen, P.-H. C.; Liu, Y.; Peng, L. How to develop machine learning models for healthcare. *Nat. Mater.* **2019**, *18*, 410−414.

(18) Gao, H.; Yu, Q.; Zhang, S. F.; Wang, T. S.; Sun, P.; Lu, H. Y.; Liu, F. M.; Yan, X.; Liu, F. M.; Liang, X. S.; Gao, Y.; Lu, G. Y. Nanosheet-assembled NiO microspheres modified by Sn^{2+} ions isovalent interstitial doping for xylene gas sensors. *Sens. Actuators, B* **2018**, *269*, 210−222.

(19) Jeong, S.-Y.; Kim, J. S.; Lee, J. H. Rational Design of Semiconductor-Based Chemiresistors and their Libraries for Next-Generation Artificial Olfaction. *Adv. Mater.* **2020**, *32*, No. 2002075.

(20) Huang, B.; Wang, Y. R.; Hu, Q.; Mu, X. M.; Zhang, Y. X.; Bai, J. L.; Wang, Q.; Sheng, Y. Z.; Zhang, Z. X.; Xie, E. Q. A low temperature and highly sensitive ethanol sensor based on Au modified In_2O_3 nanofibers by coaxial electrospinning. *J. Mater. Chem. C* **2018**, *6*, 10935−10943.

(21) Qu, J.; Ge, Y. R.; Zu, B. Y.; Li, Y. X.; Dou, X. C. Transition-Metal-Doped p-Type ZnO Nanoparticle-Based Sensory Array for Instant Discrimination of Explosive Vapors. *Small* **2016**, *12*, 1369−1377.

(22) Hu, W.; Wan, L. T.; Jian, Y. Y.; Ren, C.; Jin, K.; Su, X. H.; Bai, X. X.; Haick, H.; Yao, M. S.; Wu, W. W. Electronic Noses: From Advanced Materials to Sensors Aided with Data Processing. *Adv. Mater. Technol.* **2018**, *4*, No. 1800488.

(23) Kang, H.; Cho, S. Y.; Ryu, J.; Choi, J.; Ahn, H.; Joo, H.; Jung, H. T. Multiarray Nanopattern Electronic Nose (E-Nose) by High-Resolution Top-Down Nanolithography. *Adv. Funct. Mater.* **2020**, *30*, No. 2002486.

(24) Okur, S.; Qin, P.; Chandresh, A.; Li, C.; Zhang, Z. J.; Lemmer, U.; Heinke, L. An Enantioselective e-Nose: An array of Nanoporous Homochiral MOF Films for Stereospecific Sensing of Chiral Odors. *Angew. Chem. Int. Ed.* **2021**, *60*, 3566−3571.

(25) Mukhopadhyay, T.; Puttaraju, B.; Senanayak, S. P.; Sadhanala, A.; Friend, R.; Faber, H. A.; Anthopoulos, T. D.; Salzner, U.; Meyer, A.; Patil, S. Air-Stable n-channel Diketopyrrolopyrrole Diketopyrrolopyrrole Oligomers for High Performance Ambipolar Organic Transistors. *ACS Appl. Mater. Interfaces* **2016**, *8*, 25415−25427.

(26) Cho, S. Y.; Yoo, H. W.; Kim, J. Y.; Jung, W. B.; Jin, M. L.; Kim, J. S.; Jeon, H. J.; Jung, H. T. High-Resolution p-Type Metal Oxide Semiconductor Nanowire Array as an Ultrasensitive Sensor for Volatile Organic Compounds. *Nano Lett.* **2016**, *16*, 4508−4515.

(27) Yang, A. J.; Chu, J. F.; Li, W. J.; Wang, D. W.; Yang, X.; Lan, T. S.; Wang, X. H.; Rong, M. Z.; Koratkar, N. Short period sinusoidal

thermal modulation for quantitative identification of gas species. *Nanoscale* **2020**, *12*, 220−229.
(28) Liu, H. Y.; He, Y. H.; Nagashima, K.; Meng, G.; Dai, T. T.; Tong, B.; Deng, Z. H.; Wang, S. M.; Zhu, N. W.; Yanagida, T.; Fang, X. D. Discrimination of VOCs molecules via extracting concealed features from a temperature-modulated p-type NiO sensor. *Sens. Actuators, B* **2019**, *293*, 342−349.
(29) Hossein-Babaei, F.; Amini, A. Recognition of complex odors with a single generic tin oxide gas sensor. *Sens. Actuators, B* **2014**, *194*, 156−163.
(30) Bai, G.; Dai, H.; Deng, J.; Liu, Y.; Ji, K. Porous NiO nanoflowers and nanourchins: Highly active catalysts for toluene combustion. *Catal. Commun.* **2012**, *27*, 148−153.
(31) He, C.; Cheng, J.; Zhang, X.; Douthwaite, M.; Pattisson, S.; Hao, Z. P. Recent Advances in the Catalytic Oxidation of Volatile Organic Compounds: A Review Based on Pollutant Sorts and Sources. *Chem. Rev.* **2019**, *119*, 4471−4568.
(32) Ge, H. F.; Ding, H.; Liu, J. H. *Gas Identification by Wavelet Transform-based Fast Feature Extraction and Support Vector Machine from Temperature Modulated Semiconductor Gas Sensors*; IEEE: Seoul, South Korea, 2005; Vol. *1*−*2*, pp 1888−1891.
(33) Nakata, S.; Okunishi, H. Characteristic responses of a semiconductor gas sensor depending on the frequency of a periodic temperature change. *Appl. Surf. Sci.* **2005**, *240*, 366−374.
(34) Chen, Z. Y.; Zheng, Y. G.; Chen, K.; Li, H. Y.; Jian, J. W. Concentration Estimator of Mixed VOC Gases Using Sensor Array With Neural Networks and Decision Tree Learning. *IEEE Sens. J.* **2017**, *17*, 1884−1892.
(35) Tshitoyan, V.; Dagdelen, J.; Weston, L.; Dunn, A.; Rong, Z. Q.; Kononova, O.; Persson, K. A.; Ceder, G.; Jain, A. Unsupervised word embeddings capture latent knowledge from materials science literature. *Nature* **2019**, *571*, 95−98.
(36) Lecun, Y.; Bottou, L.; Bengio, Y.; Haffner, P. Gradient-based learning applied to document recognition. *Proc. IEEE* **1998**, *86*, 2278−2324.
(37) Sundaram, S.; Kellnhofer, P.; Li, Y. Z.; Zhu, J. Y.; Torralba, A.; Matusik, W. Learning the signatures of the human grasp using a scalable tactile glove. *Nature* **2019**, *569*, 698−702.

https://doi.org/10.1021/acssensors.1c01704
ACS Sens. XXXX, XXX, XXX−XXX